Sensors and Materials, Vol. 37, No. 5 (2025) 1915–1923
MYU Tokyo

S & M 4028

Chemical Analysis of CdMnTeSe Surface Treated with Sodium Hypochlorite and Potassium Permanganate via X-ray Photoelectron Spectroscopy

Jangwon Byun,[1†] Taejoon Mo,[2†] Younghak Kim,[3] Jiwon Seo,[4] Seungho Song,[5]
Jichul Seo,[6] Hansoo Kim,[7] Masanori Koshimizu,[8] and Beomjun Park[1,9*]

[1]Department of Materials Science and Engineering, Korea University, Seoul 02841, Republic of Korea
[2]Department of Chemical Engineering, Pohang University of Science and Technology (POSTECH),
Pohang 37673, Republic of Korea
[3]Environmental Radioactivity Assessment Team, Korea Atomic Energy Research Institute,
Daejeon 34057, Republic of Korea
[4]Department of Health and Safety Convergence Science, Korea University, Seoul 02841, Republic of Korea
[5]Department of Bioengineering, Korea University, Seoul 02841, Republic of Korea
[6]Department of Chemistry, Konkuk University, Seoul 05029, Republic of Korea
[7]Advanced Radiation Detection Instrument & Sensor Lab., Korea Atomic Energy Research Institute,
Jeongeup 56212, Republic of Korea
[8]Research Institute of Electronics, Shizuoka University, 3-5-1 Johoku, Naka-ku, Hamamatsu 432-8011, Japan
[9]The Institute for High Technology Materials and Devices, Korea University, Seoul 02841, Republic of Korea

(Received December 24, 2024; accepted March 18, 2025)

Keywords: room-temperature semiconductor detector, sodium hypochlorite, potassium permanganate, surface passivation, oxidation

We grew a $Cd_{0.95}Mn_{0.05}Te_{0.98}Se_{0.02}$ (CMTS) semiconductor, which is the next-generation gamma-ray detector operating at room temperature, via the Bridgman method. During Br etching, one of the fabrication processes for CdTe-based semiconductors, a Te-rich layer is formed on the surface of the crystal, and this Te-rich surfaces act as the charge carrier source and trapping center of photo-generated carriers. To oxidize this Te-rich layer, we introduced sodium hypochlorite (NaOCl) and potassium manganate ($KMnO_4$) into CMTS crystals, and then characterized the chemical state of the surface via X-ray photoelectron spectroscopy (XPS). The spectroscopic properties of the surface-treated CMTS were confirmed, indicating potential oxidation when precise passivation was settled.

1. Introduction

CdMnTeSe (CMTS) semiconductors are one of the promising materials for the room-temperature semiconductor detector (RTSD) operating for X/γ-ray detection.(1–3) CMTS has sufficient potential for the next-generation RTSD among the well-known CdTe-based semiconductors,(4–6) such as CdTe, CdZnTe, CdZnTeSe, and CdMnTe, owing to the following reasons: The advantages of CMTS are attributed to the homogeneous property of Mn and the

---

[†] These authors equally contributed to this work.

[*] Corresponding author: e-mail: pbj0116@korea.ac.kr

https://doi.org/10.18494/SAM5513

ISSN 0914-4935
https://myukk.org/

defect suppression of Se in the CdTe matrix during crystal growth.(1) There have been no mentioned benefits of CdZnTe yet, which is the most typical RTSD, owing to the vertically inhomogeneous distribution of zinc(7) and the high partial pressure of cadmium(8) for growth.

Despite the potential properties of CMTS, mechanical and structural defects are formed during fabrication processes.(9) This is because all CdTe-based semiconductor crystals experience the same fabrication processes regardless of their specific stoichiometry and composition. Specifically, a Te-rich surface appears during bromine-based chemical etching, excites thermal carriers/noise, and leaves the activated immobile ions acting as trapping centers for photogenerated charge carriers.(10,11) Such a non-stoichiometric surface requires passivation via oxidation in CdTe-based semiconductors. Previously, our team found the novel passivation solution based on sodium hypochlorite (NaOCl),(2,10) which guaranteed better spectral performance and potentially longer stability. Similarly, Yu *et al.*(11) have very recently reported feasible potassium-based passivants for CdZnTe (CZT), including potassium permanganate ($KMnO_4$).

In this study, we grew the CMTS ingot via the Bridgman method and processed it into planar dimensions. Afterward, we characterized the chemical state of crystal surfaces by X-ray photoelectron spectroscopy (XPS) depending on chemical treatments such as chemical etching, NaOCl passivation, and $KMnO_4$ passivation. The different oxidation results were compared and analyzed with each XPS peak of component atoms. The spectroscopic response of the CMTS detector was additionally evaluated before and after $KMnO_4$ passivation. This study will guide us for the next passivation study for CdTe-based semiconductors.

2. Materials and Methods

2.1 Crystal growth and semiconductor fabrication

A 2 inch $Cd_{0.95}Mn_{0.05}Te_{0.98}Se_{0.02}$ ingot was grown via the Bridgman method,(2) and the grown ingot was wafered with a thickness of 6.5 mm to screen the grain and twin boundaries. CMTS single crystals were extracted within the grain of the middle wafers in the CMTS ingot to clarify the typical properties of the grown CMTS crystals. The selected crystals were mechanically lapped, polished, and chemically etched with 2% Br-MeOH solution as specifically described in Ref. 12. Afterward, the $AuCl_3$ solution was selectively pipetted onto the planar CMTS crystals as shown in Fig. 1(a). The electrode deposition via the electroless method using $AuCl_3$ solution was applied for nuclear detection before and after $KMnO_4$ passivation [Fig. 1(b)], while the deposition was skipped for the CMTS sample utilized for XPS analysis. Figures 1(c) and 1(d) show the solutions used for passivation on the surface of a Br-etched CMTS crystal. Both materials were purchased from Sigma Aldrich. Both materials were weighed and made into 5% in deionized water as used in previous studies.(10,11) The passivation time was set to 5 min(11) for XPS and 3 min for nuclear detection.

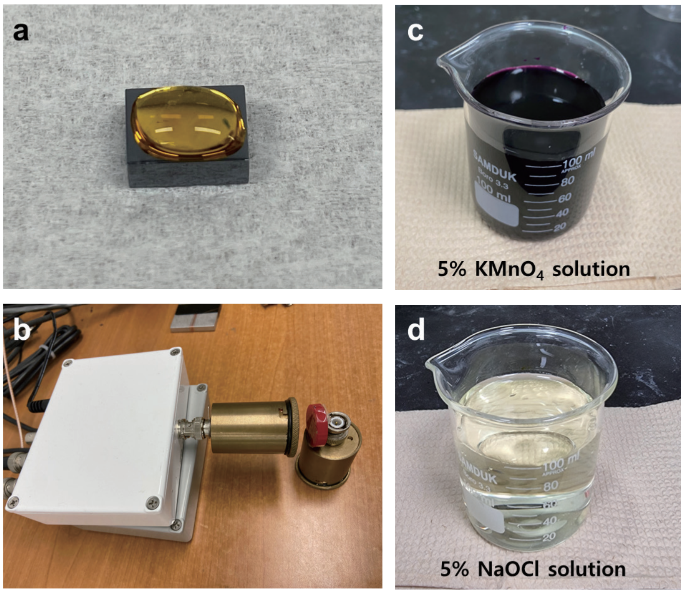

Fig. 1. (Color online) Experimental processes for fabrication and spectroscopic characterization. (a) Electroless deposition via $AuCl_3$ solution on CMTS crystal, (b) γ-ray detection with nuclear instrumentations, (c) 5% $KMnO_4$ solution, and (d) 5% NaOCl solution.

2.2 Material characterization

The binding energy of components in Br-etched/passivated CMTS was examined by XPS utilizing NEXSA (Korea Institute of Science and Technology, KIST). The analyzed atoms were Cd, Te, Mn, Se, O, and C. A microfocus monochromatic X-ray source (Al-Kα, 1486.6 eV) was used for XPS characterization with a sensitivity of 4000 k cps and a focal spot of 10−400 μm. XPS analysis was conducted under the high vacuum $< 5 \times 10^{-9}$ mbar. Planar CMTS specimens were prepared with different fabrication processes such as Br etching, $KMnO_4$ passivation, and NaOCl passivation [Figs. 1(c) and 1(d)]. The immersion times were 60 and 300 s for Br etching and both passivation processes, respectively.

2.3 Nuclear measurement

The detection scheme used is shown in Fig. 1(b). The processed CMTS detector was placed in its holder, whose signal was directly transferred to the preamplifier (CRZ-110, Cremat Inc.), shaper (CR-200, Cremat Inc.), and multichannel analyzer (Easy-MCA-8k, Amptek Inc.). The power source used was Matsusada hsx-3r5, which supplied high voltages from 100 to 300 V to the planar detector. The positive voltages were applied to the detector and gamma-rays were irradiated on the cathode side of the detector. For gamma-ray irradiation, Am-241 radioisotopes were used with a gamma-activity of 370 kBq, whose energy is 59.5 keV. The spectroscopic measurement was carried out at 25 °C to exclude the temperature-dependent variation.

3. Results and Discussion

Figure 2 presents the XPS spectra of the CdMnTeSe surface under different treatments, including only Br etching and the subsequent passivation with NaOCl and $KMnO_4$. In Fig. 2(a), the peaks at 572.5 and 582.5 eV correspond to the $3d_{5/2}$ and $3d_{3/2}$ states of Te in the CdTe lattice, respectively.(13,14) Additionally, the peaks at 573.3 and 578.3 eV represent the $3d_{5/2}$ and $3d_{3/2}$ states of atomic Te,(10,15,16) while those at 576.0 and 586.0 eV signify the $3d_{5/2}$ and $3d_{3/2}$ states of Te in TeO_2.(10,16) The spectra reveal that the Br-etched CMTS exhibits both Te peaks from CdTe and atomic Te, indicating a Te-rich surface on CdMnTeSe after Br etching [Figs. 2(a) and 2(b)]. After passivation regardless of the passivant type used, the Te metal peak disappeared, and a TeO_2 peak emerged at 576.0 eV, indicating the oxidation of atomic Te to TeO_2. As a result, the Te peak from CdTe in NaOCl-passivated CMTS appears to shift to a lower binding energy, actually owing to the disappearance of the atomic Te peak (Te(0)) located at a higher binding energy [red graph, Fig. 2(a)]. Notably, after $KMnO_4$ treatment, only TeO_2 peaks (576.0 and 586.0 eV) were left without the Te peak from CdTe. This is attributed to the potent oxidizing ability of $KMnO_4$, which can directly oxidize CdTe and atomic Te(0) on the surface.(17) $KMnO_4$ proves highly effective in oxidizing the surface compared with conventional NaOCl, while caution is advised as excessive use may lead to the direct oxidation and distortion of the CdTe lattice.

Figure 2(c) shows Cd 3d XPS peaks, indicating the chemical state of cadmium on the surface of CMTS. The Br-etched CMTS (black graph) shows a binding energy that is slightly lower than 405.3 eV, which is a typical energy for the Cd peak from CdTe.(16,18,19) It is considered as a combination of not only CdTe but also $CdBr_2$ attributed to Br etching, along with the Cd peak in

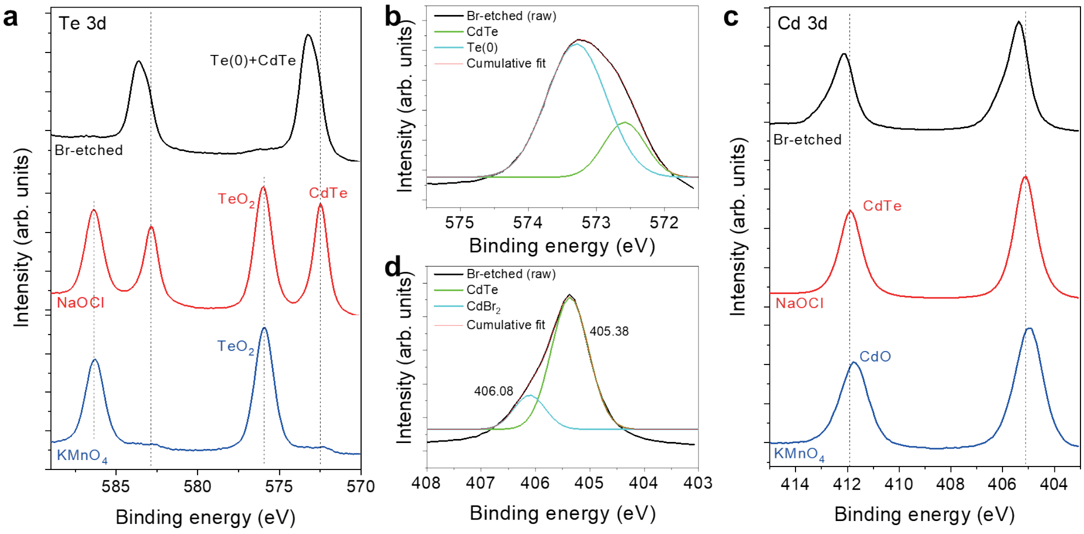

Fig. 2. (Color online) X-ray photoelectron peaks of CMTS crystals depending on the chemical treatment of surface. (a) Te 3d peaks of CMTS crystals. (b) Deconvoluted Te peak of Br-etched CMTS crystal. (c) Cd 3d peaks of CMTS crystals. (d) Deconvoluted Cd peak of Br-etched CMTS crystal.

CdTe [Fig. 2(d)]. The $CdBr_2$ peak disappeared with the introduction of NaOCl passivation, with only Gaussian-shaped Cd-Te peaks at 405.3 eV.(19) Herein, it was shown that NaOCl does not oxidize the Cd-based materials. However, the $KMnO_4$ passivation [blue graph in Fig. 2(c)] caused the shift of Cd peaks into the lower binding energy of 405.0 eV, corresponding to CdO.(20) This result indicates that the high oxidizing power of $KMnO_4$ formed CdO on the surface of CMTS, not only oxidizing the Te-rich layer. Considering the absence of Te 3d from CdTe [Fig. 2(a)], the peak area at 405.0 eV was sufficient from cadmium oxide instead of CdTe, depicting that structural distortion could occur.

Figure 3(a) illustrates the XPS spectrum of Mn 2p. In both Br etching and NaOCl passivation, the Mn $2p_{3/2}$ peak at 641.3eV is evident, signifying the presence of Mn in CMTS.(21,22) The Mn composition within stoichiometric $Cd_{0.95}Mn_{0.05}Te_{0.98}Se_{0.02}$ is too small to form the clear peak; however, previous studies(2,5) with the same composition (CMTS) also showed a lower Mn peak intensity. Additionally, the peak at 652.5 eV is composed of a convolution peak of a small quantity of Mn $2p_{1/2}$ and a dominant Cd $3p_{1/2}$ peak.(2,20) In the case of $KMnO_4$ treatment, it is observed that the presence of sufficient area of Mn peaks, as shown in the blue graph in Fig. 3(a), indicates that the $KMnO_4$ passivation not only oxidizes tellurium or cadmium but also makes Mn invade the semiconductor lattice. Figure 3(b) displays the deconvoluted Mn $2p_{3/2}$ peak of the $KMnO_4$-passivated CMTS crystal. The peak was divided into various manganese oxide peaks such as MnO, Mn_2O_3, and MnO_2, feasibly related to 640.8, 642.0, and 642.8 eV, respectively.(23–26) The areal dominance of the Mn $2p_{3/2}$ peak was in orders of MnO, Mn_2O_3, and MnO_2.

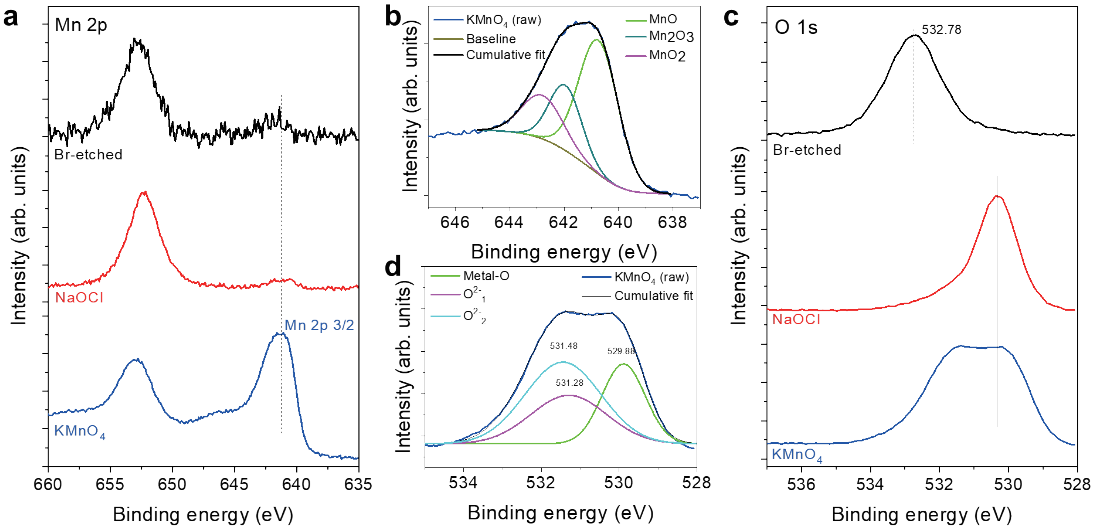

Fig. 3. (Color online) X-ray photoelectron peaks of CMTS crystals depending on the chemical treatment of surface. (a) Mn 2p peaks of CMTS crystals. (b) Deconvoluted Mn peak of $KMnO_4$-passivated CMTS crystal. (c) O 1s peaks of CMTS crystals. (d) Deconvoluted O peak of $KMnO_4$-passivated CMTS crystal.

Figure 3(c) shows the O 1s peaks of Br-etched, NaOCl-passivated, and $KMnO_4$-passivated CMTS crystals. The metal-oxide peak is typically located at approximately 530−531 eV. However, the Br-etched CMTS does not yield a detectable metal-oxide peak, which corresponds to the absence of the TeO_2 peak [Fig. 2(a)]. After the introduction of NaOCl passivation on the CMTS crystal, the treated surface exhibited a distinct peak at 530.3 eV, indicative of the metal-oxide peak, which would be attributed to TeO_2 as shown in Fig. 2(a). When CMTS was treated with $KMnO_4$ [blue graph in Fig. 3(c)], the O 1s peak represents the composite shape different from that of NaOCl-passivated CMTS. Figure 3(d) shows the deconvoluted peaks of O 1s in $KMnO_4$-passivated CMTS. Passivation with $KMnO_4$ suggests the multi-Gaussian shape of the O 1s peak, representing a summation of TeO_2, Mn oxide, and CdO.(10,20,27–29) Additionally, the peaks and components of MnOOH in O^{2-}(1) and O^{2-}(2) at higher binding energies than metal oxide correspond to an increased number of defect sites with low oxygen coordination typically observed in materials with small particles.(27–31)

Figure 4(a) illustrates the XPS spectrum of Se 3d, depending on the chemical treatment on CMTS. In the Br-etched CMTS, the spectrum reveals the presence of atomic selenium [Se(0)] alongside CdSe, which constitutes the primary selenium bond.(32–34) In post-passivation with NaOCl, the Se(0) signal diminishes, leaving predominantly bound selenium at 54.3 eV. As mentioned earlier,(32,33) passivation with $KMnO_4$ disrupts the formation of CdSe bonds, leading to the oxidation of Cd to CdO and the formation of $MnSe_2$ with no discernible peak of SeO_2.(35,36) The carbon peak of CdTe-based semiconductors is typically attributed to the carbon coating on the quartz tube for the Bridgman growth of CMTS. In the case of Se, the Br-etched CMTS reveals the presence of C-C/C-H at 284.8 eV and C with an OH group at 286.4 eV. Following

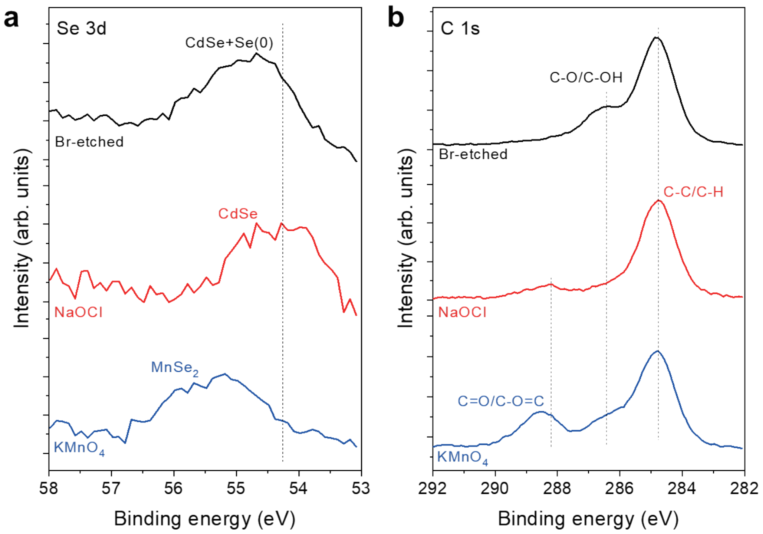

Fig. 4. (Color online) X-ray photoelectron peaks of CMTS crystals depending on the chemical treatment of surface. (a) Se 3d peaks of CMTS crystals. (b) C 1s peaks of CMTS crystals.

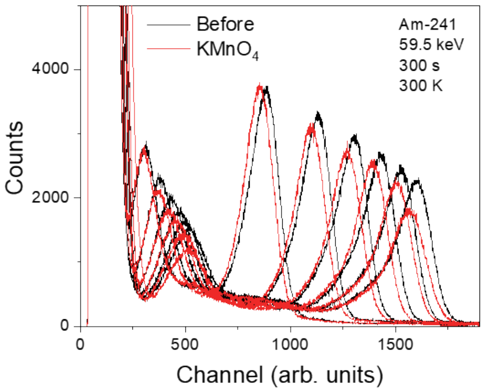

Fig. 5. (Color online) Pulse height spectra obtained with CMTS detector before/after $KMnO_4$ passivation. The physical dimensions of the CMTS detector used were 6.0 × 4.5 × 3.3 mm^3 (W×D×H).

NaOCl passivation, the OH group diminishes, and a more pronouncedly oxidized C=O/C-O=O peak emerges at 288.2 eV. Notably, with $KMnO_4$ passivation, the highest oxidizing power is observed, resulting in the robust oxidation of carbon. In contrast to other oxidants, C=O/C-O=O peak of $KMnO_4$ exhibits increased intensity.(35,37–39)

Figure 5 displays the pulse height spectra obtained using the CMTS detector before and after $KMnO_4$ passivation for 300 s. The biased voltages ranged from 100 to 300 V with a step of 50 V. The photopeak of 59.5 keV gamma-rays and the Np-L X-ray peak appeared, with the peak centroid increasing with the biased voltage regardless of the passivation process used. However, after the passivation, both peak centroids decreased differently from that indicated in a previous report;(11) We tried the same experiments three times for determining reproducibility, but results were the same. This might be from the distortion of the CdTe lattice originating from the high oxidizing power of $KMnO_4$ to oxide not only tellurium but also cadmium/manganese. However, the previous study suggested that $KMnO_4$-based passivation successfully improved the spectroscopic performance of CZT.(11) Although the composition of CZT is slightly different from that of CMTS used in this study, the passivation mechanism is primarily attributed to the oxidation of tellurium, indicating similarities in performance enhancements. Thus, the passivation process via $KMnO_4$ requires fine and precise optimization; however, $KMnO_4$ has the potential to be applied as a good passivant due to its strong oxidation and formation of TeO_2 without atomic Te(0).

4. Conclusion

In this study, we investigated the surface passivation effects of NaOCl and $KMnO_4$ on CMTS crystals, with a specific focus on their chemical and structural impacts. NaOCl effectively oxidized a Te-rich layer without introducing significant lattice distortions, making it a reliable passivant for maintaining detector performance.(2) In contrast, $KMnO_4$, while demonstrating superior oxidizing capability, led to the formation of CdO and Mn-based oxides, as well as the partial oxidation of the CdTe lattice, resulting in structural distortions that negatively affected spectroscopic performance. These findings highlight the necessity of the precise optimization of the $KMnO_4$ passivation process to balance its high oxidizing power with the preservation of lattice integrity, thereby ensuring a potential passivation effect for improved detector performance.

Conflict of Interest

The authors do not have any conflicts of interest to declare.

Acknowledgments

This work was supported by the National Research Foundation of Korea (NRF) grant funded by the Korea government (MSIT) (RS-2025-00513114), supported by the KAERI Institutional Program (Project No. 522610-24), and technically supported by the Radiation Equipment FAB in the KAERI (No. 2710007334).

References

1 J. Byun, T. Mo, H. Yuk, G. Heo, J. Seo, H. Kim, and B. Park: Mater. Lett. **359** (2024) 135970. https://doi.org/10.1016/j.matlet.2024.135970

2 Y. Kim, J. Ko, J. Byun, J. Seo, and B. Park: Appl. Radiat. Isot. **200** (2023) 110914. https://doi.org/10.1016/j.apradiso.2023.110914

3 A. Masłowska, D. M. Kochanowska, A. Sulich, J. Z. Domagala, M. Dopierała, M. Kochański, M. Szot, W. Chromiński, and A. Mycielski: Sensors (Basel) **24** (2024) 2. https://doi.org/10.3390/s24020345

4 T. Takahashi and S. Watanabe: IEEE Trans. Nucl. Sci. **48** (2001) 4. https://doi.org/10.1109/23.958705

5 K. Kim, S. Cho, J. Suh, J. Hong, and S. Kim: IEEE Trans. Nucl. Sci. **56** (2009) 3. https://doi.org/10.1109/TNS.2009.2015662

6 U. N. Roy, G. S. Camarda, Y. Cui, R. Gul, G. Yang, J. Zazvorka, and R. B. James: Sci. Rep. **9** (2019) 1. https://doi.org/10.1038/s41598-019-43778-3

7 N. Zhang, A. Yeckel, A. Burger, Y. Cui, K. G. Lynn, and J. J. Derby: J. Cryst. Growth **325** (2011) 1. https://doi.org/10.1016/j.jcrysgro.2011.04.041

8 W. Wei, W. Jin, J. Luo, L. Lv, and G. Li: J. Appl. Phys. **136** (2024) 22. https://doi.org/10.1063/5.0242654

9 Q. Zheng, F. Dierre, J. Crocco, V. Carcelen, H. Bensalah, J. H. Plaza, and E. Dieguez: Appl. Surf. Sci. **257** (2011) 20. https://doi.org/10.1016/j.apsusc.2011.05.098

10 B. Park, Y. Kim, J. Seo, J. Byun, and K. Kim: Nucl. Eng. Technol. **54** (2022) 12. https://doi.org/10.1016/j.net.2022.06.005

11 P. Yu, G. Yang, X. Sun, T. Rao, H. Fu, L. Luan, and H. Li: Nucl. Instrum. Methods Phys. Res. A **1051** (2023) 168229. https://doi.org/10.1016/j.nima.2023.168229

12 B. Park, K. Jung, and C. Kim: J. Radiat. Prot. Res. **49** (2024) 2. https://doi.org/10.14407/jrpr.2024.00073

13 A. D. Compaan, X. Deng, and R. G. Bohn: NREL NREL/SR–520–27666 (2000). https://doi.org/10.2172/754623

14 G. Zhang, Y. Yao, X. Wang, Z. Li, Y. Song, H. Wu, W. Chen, Y. Tang, H. Shen, and X. Huang: J. Mater. Chem. A **2** (2014) 16. https://doi.org/10.1039/C3TA14539E

15 C. J. Powell: J. Electron Spectros. Relat. Phenomena **185** (2012) 1. https://doi.org/10.1016/j.elspec.2011.12.001

16 K. T. Chen, D. T. Shi, H. Chen, B. Granderson, M. A. George, W. E. Collins, A. Burger, and R. B. James: J. Vac. Sci. Technol. A **15** (1997) 3. https://doi.org/10.1116/1.580719

17 Z. Wang, J. Li, B. Liu, J. Hu, X. Yao, and J. Li: J. Phys. Chem. B **109** (2005) 49. https://doi.org/10.1021/jp055023k

18 H. T. Masood, Z. Muhammad, M. Habib, D. M. Wang, and D. L. Wang: Chin. Phys. B **26** (2017) 6. https://doi.org/10.1088/1674–1056/26/6/067503

19 M. Shen, W. Jia, Y. You, Y. Hu, F. Li, S. Tian, and D. Han: Nanoscale Res. Lett. **8** (2013) 1. https://doi.org/10.1186/1556-276X-8-253

20 D. J. Jeejamol, K. S. Jai Aultrin, and M. Dev Anand: Opt. Quantum Electron. **54** (2022) 5. https://doi.org/10.1007/s11082-022-03694-9

21 J. Tian, L. Lv, C. Fei, Y. Wang, X. Liu, and G. Cao: J. Mater. Chem. A **2** (2014) 46. https://doi.org/10.1039/C4TA04534C

22 M. Wang, K. Chen, J. Liu, Q. He, G. Li, and F. Li: Catalysts **8** (2018) 4. https://doi.org/10.3390/catal8040138

23 V. Di Castro and G. Polzonetti: J. Electron Spectros. Relat. Phenomena **48** (1989) 1. https://doi.org/10.1016/0368–2048(89)80009–X

24 E. S. Ilton, J. E. Post, P. J. Heaney, F. T. Ling, and S. N. Kerisit: Appl. Surf. Sci. **366** (2016) 475. https://doi.org/10.1016/j.apsusc.2015.12.159

25 M. C. Biesinger, L. W. Lau, A. R. Gerson, and R. S. C. Smart: Appl. Surf. Sci. **257** (2010) 3. https://doi.org/10.1016/j.apsusc.2010.07.086

26 M. C. Militello and S. W. Gaarenstroom: Surf. Sci. Spectra **8** (2001) 3. https://doi.org/10.1116/11.20020401

27 C. Shang, X. Yang, G. Hu, Y. Sun, L. Chen, P. Zhang, M. Wang, J. Wang, H. Zhao, Q. Zhang, X. Huang, Z. Huang, Y. Zhu, and X. Yang: Sci. China Mater. **10** (2017) 60. https://doi.org/10.1007/s40843-017-9103-1

28 C. Yuan, J. Li, L. Hou, X. Zhang, L. Shen, and X. W. Lou: Adv. Funct. Mater. **22** (2012) 21. https://doi.org/10.1002/adfm.201200994

29 B. R. Strohmeier and D. M. Hercules: J. Phys. Chem. **88** (1984) 21. https://doi.org/10.1021/j150664a041

30 K. Meng, X. Wu, X. Zhang, S. Su, Z. Huang, X. Min, F. Peng, Z. Zhou, and M. Fang: ACS Omega **4** (2019) 20. https://doi.org/10.1021/acsomega.9b02431

31 C. Shang, X. Yang, Z. Wang, M. Li, M. Liu, J. Zhu, H. Huang, X. Wu, Y. Chen, and Z. Lu: Sci. China Mater. **10** (2017) 60. https://doi.org/10.1007/s40843-017-9103-1

32 M. Y. Huang, X. B. Li, Y. J. Gao, J. Li, H. L. Wu, L. P. Zhang, B. Chen, C. H. Tung, and L. Z. Wu: J. Mater. Chem. A **6** (2018) 14. https://doi.org/10.1039/C8TA00385H

33 E. Ebrahimi, M. Irfan, F. Shabani, Y. Kocak, B. Karakurt, E. Erdem, E. Dogan, E. Yildiz, and E. Ozensoy: ChemCatChem **12** (2020) 24. https://doi.org/10.1002/cctc.202000749

34 M. Shenasa, S. Sainkar, and D. Lichtman: J. Electron Spectros. Relat. Phenomena **40** (1986) 4. https://doi.org/10.1016/0368-2048(86)80043-3

35 B. Balamuralitharan, S. N. Karthick, S. K. Balasingam, K. V. Hemalatha, S. Selvam, J. A. Raj, K. Prabakar, Y. Jun, and H. J. Kim: Energy Technol. **5** (2017) 1953. https://doi.org/10.1002/ente.201700097

36 H. Liang, L. Cao, L. Li, J. Duap, X. Liao, F. Long, J. Zhou, Y. Xiao, Y.-J. Zeng, and S. Zhou: Mater. Horiz. **8** (2021) 1286. https://doi.org/10.1039/d1mh00009h

37 X. Chen, X. Wang, and D. Fang: Fuller. Nanotub. Car. N. **28** (2020) 1048. https://doi.org/10.1080/1536383X.2020.1794851

38 A. V. Shchukarev and D. V. Korolkov: Cent. Eur. J. Chem. **2** (2004) 347. https://doi.org/10.2478/BF02475578

39 A. Dolgov, D. Lopaev, C. J. Lee, E. Zoethout, V. Medvedev, O. Yakushev, and F. Bijkerk: Appl. Surf. Sci. **353** (2015) 708. https://doi.org/10.1016/j.apsusc.2015.06.079